Supporting Information

Photolithography-Assisted Precise Patterning of Nanocracks for Ultrasensitive Strain Sensors

Junshan Liu, Hongji Guo, Ming Li, Chi Zhang, Yongzhi Chu, Lixuan Che, Zhihao Zhang, Rui Li, Jining Sun, Yao Lu**

Prof. J. Liu, H. Guo, C. Zhang, Y. Chu, Z. Zhang, Prof. J. Sun
Key Laboratory for Micro/Nano Technology and System of Liaoning Province, Dalian University of Technology, Dalian, Liaoning, 116024, China.
E-mail: liujs@dlut.edu.cn (J. Liu)

Prof. J. Liu
Key Laboratory for Precision and Non-traditional Machining Technology of Ministry of Education, Dalian University of Technology, Dalian, Liaoning, 116024, China.

Prof. M. Li, L. Che, Prof. R. Li
State Key Laboratory of Structural Analysis for Industrial Equipment, Department of Engineering Mechanics, Dalian University of Technology, Dalian, Liaoning, 116024, China.

Dr. Y. Lu
Department of Chemistry, School of Biological and Chemical Sciences, Queen Mary University of London, London E1 4NS, UK.
E-mail: yao.lu@qmul.ac.uk (Y. Lu)

Theory Section

Estimation of Strains for Exposed and Unexposed Au Films

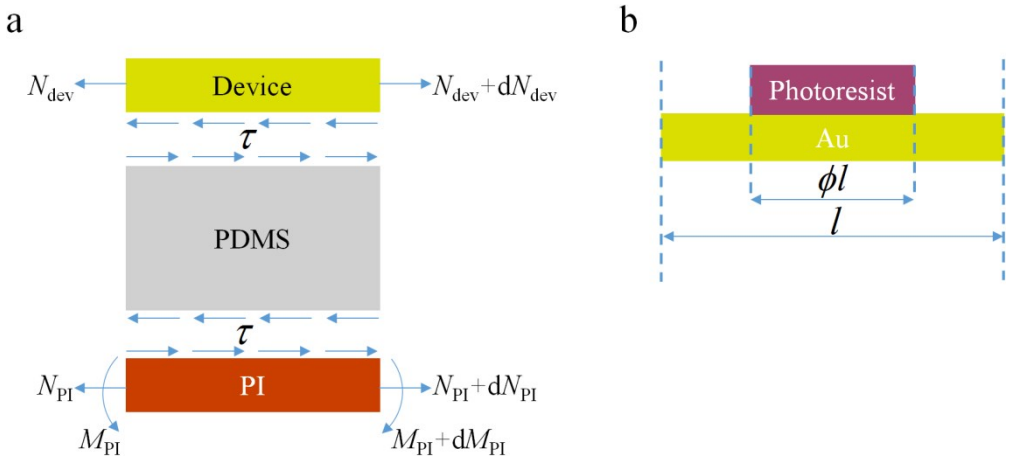

Figure S1. Shear lag model to estimate strains in both exposed and unexposed Au films**.** (a) Schematic diagram of shear lag model considering a device layer with an effective tensile rigidity. (b) The non-uniform device layer can be divided into two parts: exposed Au film and composite consisting of the photoresist layer and the unexposed Au film.

A shear lag model is developed to estimate strains in both exposed and unexposed Au films mounted on a compliant PDMS substrate in the four-layer structure (Figure 1d).[S1,S2] As illustrated in Figure S1a, the PI layer is modeled as an elastic beam sustaining both stretching and bending loads, and the compliant and thick PDMS layer is modeled as a shear lag to transmit non-uniform shear stress τ between the PI layer and the device layer. As illustrated in Figure S1b, a non-uniform device layer can be divided into two periodically distributed parts: exposed Au film and composite consisting of unexposed Au film and photoresist layer. For composite, the tensile rigidity is $\bar{E}_{comp}h_{comp} = \bar{E}_{Pr}h_{Pr} + \bar{E}_{Au}h_{Au}$, in which $\bar{E}_{\mathrm{Pr}}, \bar{E}_{\mathrm{Au}}, h_{\mathrm{Pr}}$ and h_{Au} denote the plane-strain modulus and thickness for the photoresist layer and unexposed Au film, respectively. For the sake of simplification, in our shear lag model, the device layer in Figure S1b is treated as a uniform layer, the effective tensile rigidity is $\bar{E}_{dev}h_{dev} = \bar{E}_{comp}h_{comp}\bar{E}_{Au}h_{Au}/\left[(1-\phi)\bar{E}_{comp}h_{comp} + \phi\bar{E}_{Au}h_{Au}\right]$, in which ϕrepresents the length

fraction of composite in the non-uniform device layer as illustrated in Figure S1b. The device layer becomes a uniform Au film when ϕ approaches 0.

The force and moment equilibrium equations for the device layer and PI layer as illustrated in Figure S1a are

$$\frac{dN_{dev}}{dx} - \tau = 0 \;, \frac{dN_{PI}}{dx} + \tau = 0 \;, \frac{dM_{PI}}{dx} + \frac{\tau h_{PI}}{2} = 0 \tag{S1}$$

in which N_{dev} and N_{PI} are axial forces for the device layer and the PI layer, M_{PI} and τ are bending moment in the PI layer and the non-uniform shear stress transmitted by the PDMS layer, respectively. The force and moments can be related to the displacements as

$$N_{dev} = \bar{E}_{dev} h_{dev} \frac{du_{dev}}{dx} \;, N_{PI} = \bar{E}_{PI} h_{PI} \frac{du_{PI}}{dx} \;, M_{PI} = -\frac{\bar{E}_{PI} {h_{PI}}^3 d^2 \omega_{PI}}{12 \quad dx^2} \tag{S2}$$

where $\bar{E}_{PI} = E_{PI}/\left(1 - \nu_{PI}^2\right)$ denotes the plane-strain modulus of the PI layer, the device layer has an axial displacement u_{dev}, while u_{PI} and ω_{PI} represent the axial and lateral displacements in the PI layer, respectively.

The shear stress τ between the device layer and the PI layer is a function of displacements in the device layer and the PI layer as

$$\tau = \frac{G_{PDMS}}{h_{PDMS}} \left[u_{dev} - u_{PI} + \left(h_{PDMS} + \frac{h_{PI}}{2} \right) \frac{d\omega_{PI}}{dx} \right] \tag{S3}$$

in which G_{PDMS} is the shear modulus of the compliant PDMS layer.

Substituting Equation (S1) and (S2) into the second derivative of Equation (S3), yielding an ordinary differential equation as

$$\frac{d^2\tau}{dx^2} - \frac{G_{PDMS}}{h_{PDMS}} \left(\frac{1}{\bar{E}_{dev} h_{dev}} + \frac{4}{\bar{E}_{PI} h_{PI}} + \frac{6 h_{PDMS}}{\bar{E}_{PI} {h_{PI}}^2} \right) \tau = 0 \tag{S4}$$

For the four-layer structure as illustrated in Figure 1d, the bottom PI layer is stretched by a weight W while the four-layer structure is bent on a stainless tube with a radius of curvature of ρ = 4 mm. Therefore, the boundary conditions of the shear lag model are

$$
\begin{aligned}
x = \pm L, & \quad N_{dev} = 0 \\
x = \pm L, & \quad N_{PI} = W \\
x = \pm L, & \quad M_{PI} = \frac{\bar{E}_{PI} h_{PI}^{\ 3}}{12} \frac{1}{\rho + \frac{h_{PI}}{2}}
\end{aligned}
\tag{S5}
$$

in which L represents the half-length of the device layer. Finally, we can determine the shear stress τ as

$$
\tau = -\frac{\alpha \sinh(\beta x)}{\beta \cosh(\beta L)} \tag{S6}
$$

where $\alpha = \frac{G_{PDMS}}{h_{PDMS}} \left[\frac{W}{\bar{E}_{PI} h_{PI}} + \frac{2h_{PDMS} + h_{PI}}{2\rho + h_{PI}} \right]$ and $\beta = \sqrt{\frac{G_{PDMS}}{h_{PDMS}} \left(\frac{1}{\bar{E}_{dev} h_{dev}} + \frac{4}{\bar{E}_{PI} h_{PI}} + \frac{6h_{PDMS}}{\bar{E}_{PI} h_{PI}^{\ 2}} \right)}$.

The membrane strain $\varepsilon_{dev} = du_{dev}/dx$ is

$$
\varepsilon_{dev} = \frac{-1}{\bar{E}_{dev} h_{dev}} \int_x^L \tau dx = \frac{\alpha}{\beta^2 \bar{E}_{dev} h_{dev}} \frac{\cosh(\beta L) - \cosh(\beta x)}{\cosh(\beta L)} \tag{S7}
$$

which yields an effective mean strain to the device layer as.

$$
\varepsilon_{dev}^{eff} = \frac{1}{L} \int_0^L \varepsilon_{dev} dx = \frac{\alpha}{\beta^2 \bar{E}_{dev} h_{dev}} \left[1 - \frac{\tanh(\beta L)}{\beta L} \right] \tag{S8}
$$

By applying this effective strain to the non-uniform device layer as illustrated in Figure S1b, different tensile rigidities in the exposed and unexposed Au film regions lead to the strain re-distribution. Simply, we can have $\varepsilon_{Au}^{unexposed} = \bar{E}_{dev} h_{dev} \varepsilon_{dev}^{eff} / \bar{E}_{comp} h_{comp}$ and $\varepsilon_{Au}^{exposed} = \bar{E}_{dev} h_{dev} \varepsilon_{dev}^{eff} / \bar{E}_{Au} h_{Au}$, in which β is a function of the length fraction $\emptyset$.

For the four-layer structure as shown in Figure 1d, we have $E_{\mathrm{PI}} = 3$ GPa, $v_{\mathrm{PI}} = 0.3$, $h_{\mathrm{PI}} = 75$ um, $E_{\mathrm{PDMS}} = 1$ MPa, $v_{\mathrm{PDMS}} = 0.46$, $h_{\mathrm{PDMS}} = 1$ Mm, $E_{Au} = 82$ GPa, $v_{\mathrm{Au}} = 0.42$, h_{Au}=50 nm, and $E_{\mathrm{Pr}} = 7.5$ GPa, $v_{\mathrm{PI}} = 0.28$, $h_{\mathrm{Pr}} = 4.6$ um, The half-length of the device layer is $L = 5$ mm, the tensile load $W = 0.2$ N is caused by the 20 g weight and the radius of curvature $\rho = 4$ mm.

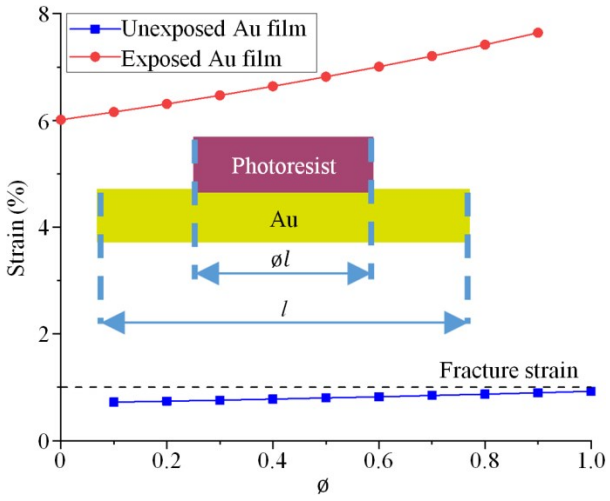

Figure S2. Strains in both exposed and unexposed Au films with varying length fractions ø obtained from mechanics model.

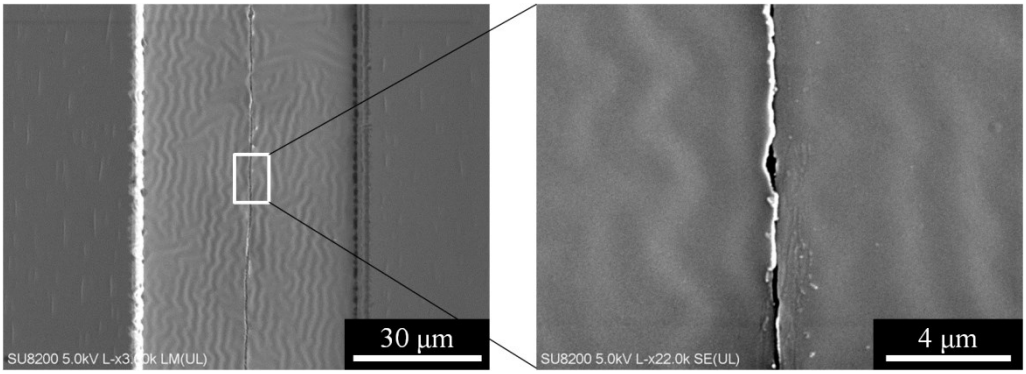

Figure S3. SEM images of straight Cu nanocracks with an average width smaller than 100 nm.

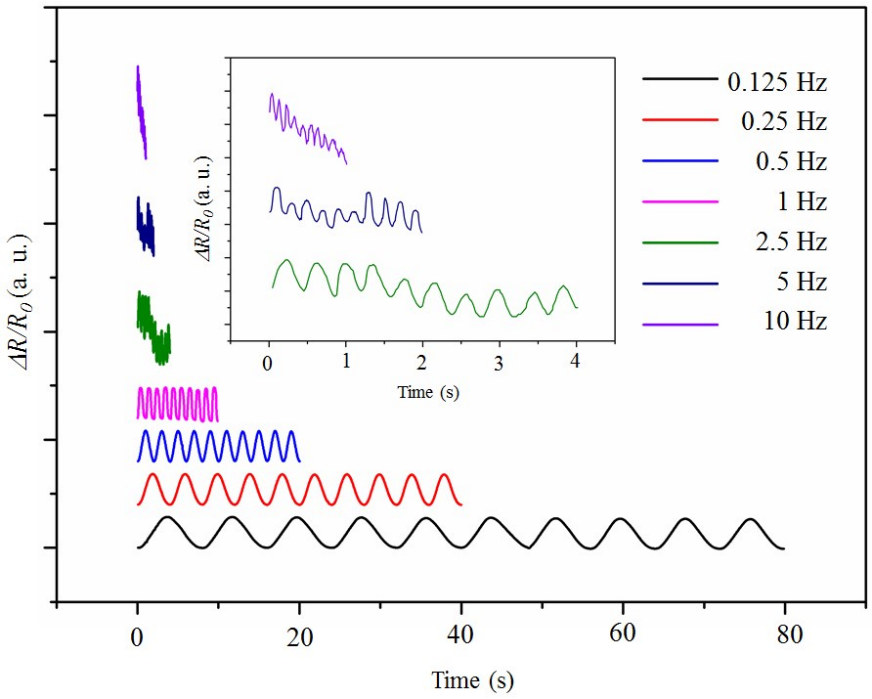

Figure S4. Dynamic response curves of the Au/PDMS nCBSS in 0-1% strain range.

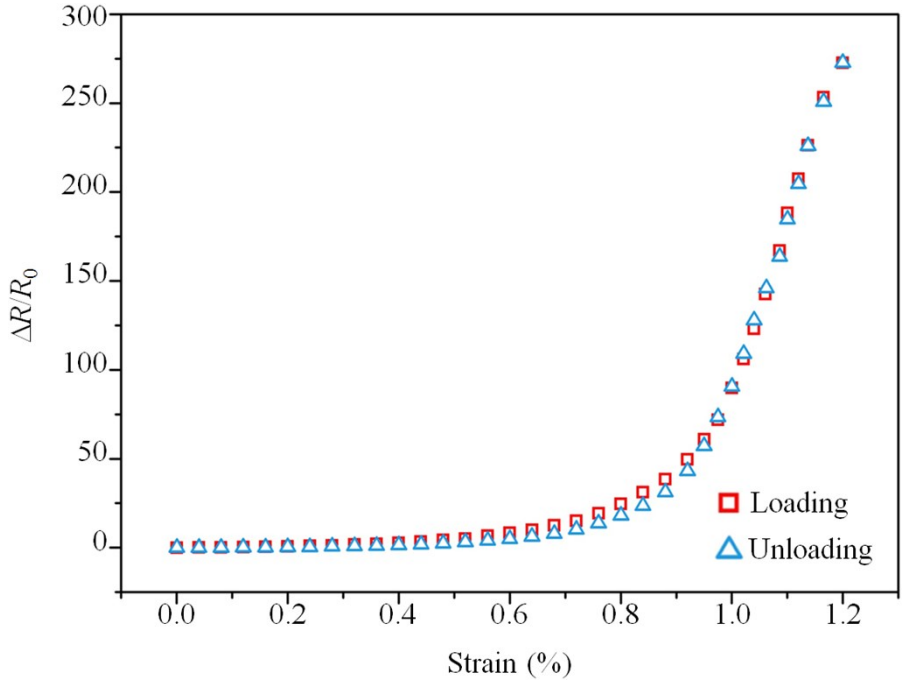

Figure S5. Hysteresis test of the Au/PDMS nCBSS at a speed of 0.1 mm/min.

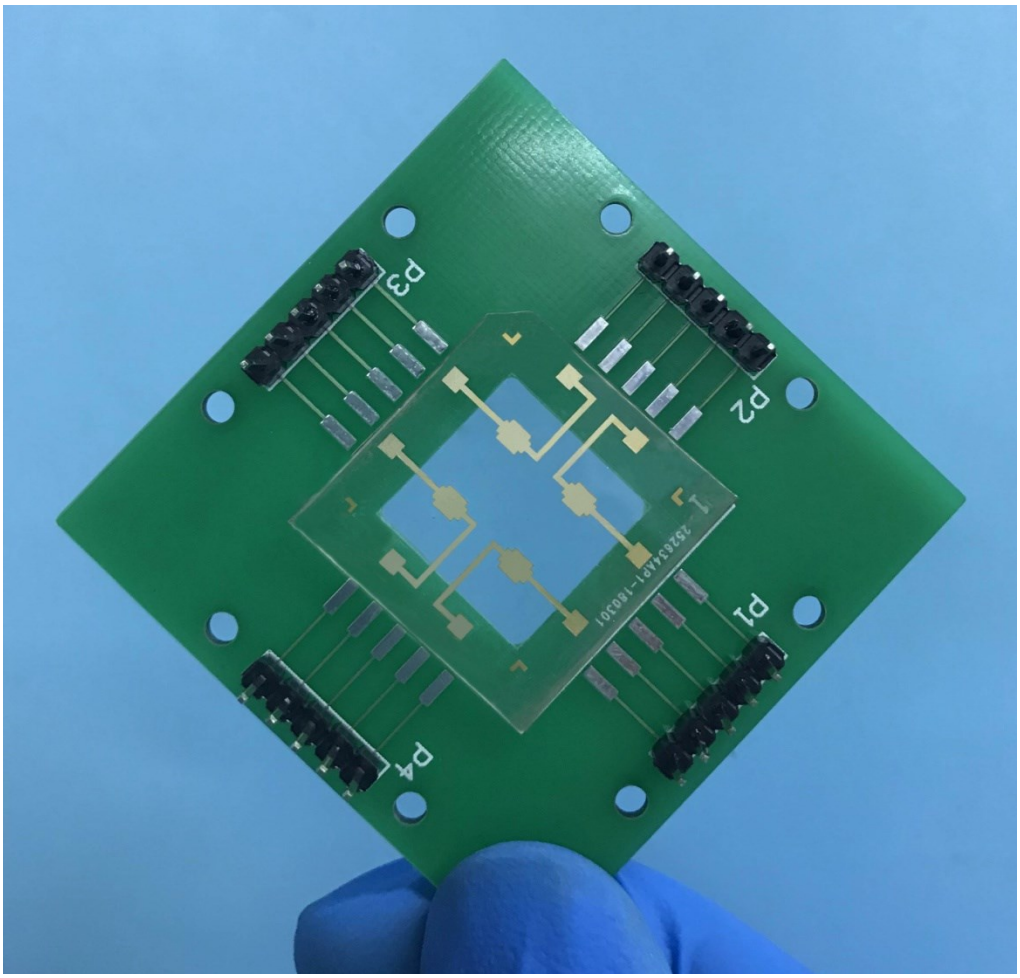

Figure S6. The 2 × 2 array of the Au/PDMS nCBSS.

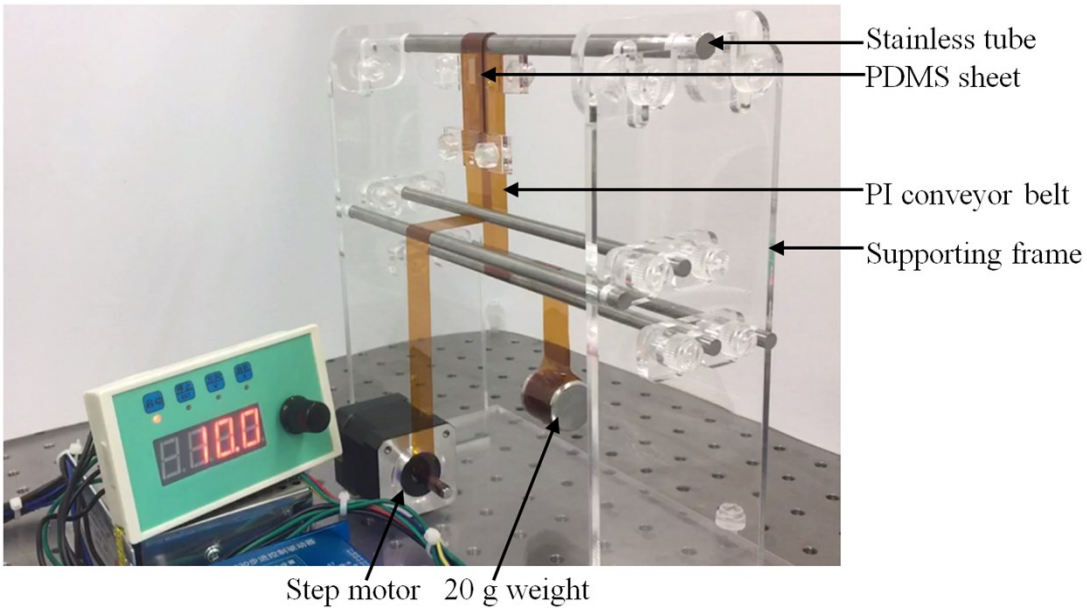

Figure S7. The homemade equipment for bending the PDMS sheet.

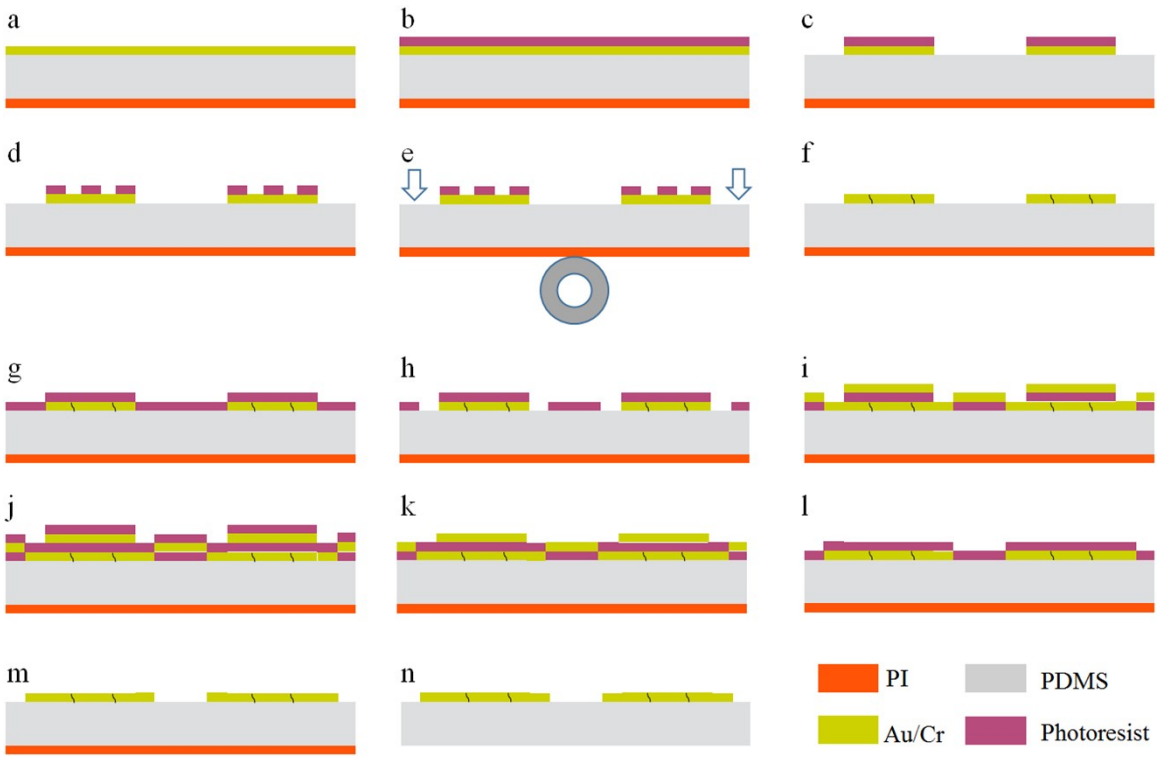

Figure S8. Fabrication of the 2 × 2 array of the Au/PDMS nCBSS. (a) Adhere the PDMS sheet to a PI film and sputter a Cr film and an Au film. (b) Spin-coat a positive photoresist. (c) Pattern the photoresist. (d) Etch the exposed gold and chromium. (e) Bend the PDMS sheet. (f) Remove the photoresist. (g) Spin-coat a positive photoresist. (h) Patten the photoresist. (i) Sputter a Cr film and an Au film. (j) Spin-coat a positive photoresist. (k) Patten the photoresist. (l) Etch the exposed gold and chromium. (m) Remove the photoresist. (m) Detach the PDMS sheet from the PI film.

Table S1 Comparison of the GFs of different nCBSSs in 0-1.2% strain range

Materials	Crack patterning methods	Sensitivity (GF_{Max})	Stretchability (%)	Sensitivity (1.2% strain)	Ref.
Pt/PUA[a)]	Directly bending	2000	2	980	S3
Au/PET	Directly stretching	1600	2	1628	S4
ITO[b)]/PET	Directly stretching	4000	2	918	S5
Pt/PUA	Directly bending	2000	2	2500	S6
PEDOT:PSS[c)] /PDMS	Directly stretching	1100	2	436	S7
Au/PI	Directly stretching	10000	2	2943	S8
AgNws[d)] /TPU	Directly stretching	1108.91	1.5	484	S9
Pt/PUA	Directly bending	16000	2	4535	S10
Au/PUA	Stress concentrating	2×10^6	10	992	S11
Au/PDMS	Directly stretching	5888.59	2	793	S12
Au/PI	Directly stretching	650	2	571	S13
CNT-KH550[e)]/PDMS	Directly stretching	1280	2	1632	S14
rGO[f)]/PDMS	Directly stretching	466	10	158	S15
Pt/PDMS	Directly stretching	1560	2	712	S16
Au/PDMS	Directly stretching	5000	1	------	S17
Au/PDMS	Directly stretching	5000	1	------	S18
Au/PDMS	PAnCP	19883	1.2	19883	This work

[a)] PUA (polyurethane acrylate); [b)] ITO (indium tin oxide); [c)] PEDOT: PSS (poly (3,4-ethylenedioxythiophene): poly(4-styrene sulfonatesulfonate); [d)] AgNws (silver nanowires); [e)] KH550 (3-aminopropyltriethoxysilane); [f)] rGO (reduced graphene oxide).

References

[S1] H. Cheng, J. Wu, M. Li, D. H. Kim, Y. S. Kim, Y. Huang, Z. Kang, K. C. Hwang, J. A. Rogers, *Appl. Phys. Lett.* **2011,** 98, 061902.

[S2] J. Wu, M. Li, W. Chen, D. H. Kim, Y. S. Kim, Y. Huang, K. C. Hwang, Z. Kang, J. A. Rogers, *Acta Mech. Sin.* **2010,** 26, 881.

[S3] D. Kang, P. V. Pikhitsa, Y. W. Choi, C. Lee, S. S. Shin, L. Piao, B. Park, K. Y. Suh, T. i. Kim, M. Choi, *Nature* **2014,** 516, 222.

[S4] T. Lee, Y. W. Choi, G. Lee, S. M. Kim, D. Kang, M. Choi, *RSC Adv.* **2017,** 7, 34810.

[S5] T. Lee, Y. W. Choi, G. Lee, P.V. Pikhitsa, D. Kang, S. M. Kim, M. Choi, *J. Mater. Chem. C* **2016**, 4, 9947.

[S6] B. Park, S. Lee, H. Choi, J. U. Kim, H. Hong, C. Jeong, D. Kang, T. i. Kim, *Nanoscale* **2018**, 10, 4354.

[S7] H. Wu, Q. Liu, W. Du, C. Li, G. Shi, *ACS Appl. Mater. Interfaces* **2018,** 10, 3895.

[S8] T. Kim, T. Lee, G. Lee, Y. W. Choi, S. M. Kim, D. Kang, M. Choi, *Appl. Sci.* **2018,** 8, 367.

[S9] S. Chen, Y. Wei, S. Wei, Y. Lin, L. Liu, *ACS Appl. Mater. Interfaces* **2016**, 8, 25563.

[S10] B. Park, J. Kim, D. Kang, C. Jeong, K. S. Kim, J. U. Kim, P. J Yoo, T. i. Kim, *Adv. Mater.* **2016**, 28, 8130.

[S11] Y. W. Choi, D. Kang, P. V. Pikhitsa, T. Lee, S. M. Kim, G. Lee, D. Tahk, M. Choi, *Sci. Rep.* **2017**, 7, 40116.

[S12] Z. Han, L. Liu, J. Zhang, Q. Han, K. Wang, H. Song, Z. Wang, Z. Jiao, S. Niu, L. Ren, *Nanoscale* **2018**, 10, 15178.

[S13] M. Kim, H. Choi, T. Kim, I. Hong, Y. Roh, J. Park, S. Seo, S. Han, J. s. Koh, D. Kang, *Materials* **2019,** 12, 1516.

[S14] X. Zhou, L. Zhu, L. Fan, H. Deng, Q. Fu, *ACS Appl. Mater. Interfaces* **2018**, 10, 31655.

[S15] T. Sakorikar, M. K. Kavitha, P. Vayalamkuzhi, M. Jaiswal, *Sci. Rep.* **2017**, 7, 2598.

[S16] H. H. Hsieh, F. C. Hsu, Y. F. Chen, *ACS Sens.* **2018**, 3, 113.

[S17] T. Yang, X. Li, X. Jiang, S. Lin, J. Lao, J. Shi, Z. Zhen, Z. Li, H. Zhu, *Mater. Horiz.* **2016**, 3, 248.

[S18] C. Wang, J. Zhao, C. Ma, J. R. Sun, L. Tian, X. Li, F. Li, X. Han, C. Liu, C. Shen, L. Dong, J. Yang, C. Pan, *Nano Energy* **2017**, 34, 578.